

**Strong field line shapes and photon statistics from a single molecule under anomalous noise**

František Šanda

*Faculty of Mathematics and Physics, Charles University, Ke Karlovu 5, Prague 121 16, Czech Republic*

(Received 4 June 2009; published 28 October 2009)

We revisit the line-shape theory of a single molecule with anomalous stochastic spectral diffusion. Waiting time profiles for bath induced spectral jumps in the ground and excited states become different when a molecule, probed by continuous-wave laser field, reaches the steady state. This effect is studied for the stationary dichotomic continuous-time-random-walk spectral diffusion of a single two-level chromophore with power-law distributions of waiting times. Correlated waiting time distributions, line shapes, two-point fluorescence correlation function, and Mandel  $Q$  parameter are calculated for arbitrary magnitude of laser field. We extended previous weak field results and examined the breakdown of the central limit theorem in photon statistics, indicated by asymptotic power-law growth of Mandel  $Q$  parameter. Frequency profile of the Mandel  $Q$  parameter identifies the peaks of spectrum, which are related to anomalous spectral diffusion dynamics.

DOI: [10.1103/PhysRevE.80.041132](https://doi.org/10.1103/PhysRevE.80.041132)

PACS number(s): 05.40.Fb, 42.50.Ar

**I. INTRODUCTION**

Single molecule experiments rapidly expanded our knowledge about optical properties of biomolecules, organic dyes, and quantum dots by focusing on distributions and fluctuations of molecular parameters rather than ensemble averages [1–4]. It posed a significant simulation challenge at both phenomenologic and *ab initio* levels [5,6]. Statistics of on-off blinking times in single CdSe quantum dots [7] and fluorescence correlations of proteins [8] or organic dyes [9] showed broad range of dynamical time scales in optical response from single molecules, microscopic origin of which remains still under debate [10–13]. Sophisticated control of multipoint correlations was instrumental to determine underlying fractional Gaussian [14] and continuous-time-random-walk (CTRW) [15,16] dynamics of fluorescence rates in biomolecules and quantum dots, respectively.

Structural information from the fluorescence trace is conveniently extracted into the kinetic schemes [17,18]. Unraveling rate fluctuations into the dynamics of the transition frequency makes one step beyond the prevailing framework. Weak field line shapes of molecules with anomalous CTRW spectral diffusion can be approached by ground-state multipoint dipole correlation function within the response function (perturbation) theory [19,20]. Theory of strong field line shapes and photon counting statistics based on the Bloch optical equations [21] and generating function method [22,23] can be easily extended to account for the Markovian spectral diffusion [24–26]. Treatment of CTRW noise, however, requires careful inspection of the steady state beyond the master equation approach [27,28] or the perturbation theory. Consistent theory of strong field anomalous line shapes, which accounts for the initial steady-state correlations between the bath dynamics and the Liouville space quantum dynamics, is the goal of this paper.

The paper is organized as follows: The CTRW model of spectral diffusion will be summarized in Sec. II. The line shapes and the two-point correlation functions for emission from the two-level chromophore driven by continuous-wave (CW) laser field will be calculated in Secs. III and IV. Finally, the steady-state correlations between the state of chro-

mophore and the spectral diffusion will be shown explicitly by calculating the probability density functions for first spectral jump in the ground and in the excited state (Sec. V).

**II. CONTINUOUS TIME RANDOM WALKS SPECTRAL DIFFUSION**

The dichotomic CTRW model of spectral diffusion [19,28,29] assumes that jumps between two bath states  $u$  and  $d$  come randomly, with the waiting time probability densities (WTDs)  $\psi_u(t)$  and  $\psi_d(t)$  for the jump from  $u$  to  $d$  and vice versa, respectively. At the time of jump all memory is erased (renewal) and the waiting times for the subsequent jumps are not correlated. This renewal property makes the model solvable. The WTDs will be organized into a matrix in the space of bath states  $(u, d)$ ,

$$\Psi(t) = \begin{pmatrix} 0 & \psi_d(t) \\ \psi_u(t) & 0 \end{pmatrix}. \quad (1)$$

Diagonal matrix of survival functions

$$\Phi(t) = \begin{pmatrix} \phi_u(t) & 0 \\ 0 & \phi_d(t) \end{pmatrix} \quad (2)$$

describes the probability  $\phi_{u,d}(t) \equiv \int_t^\infty \psi_{u,d}(t') dt'$  to persist in the bath state without jump from the time of renewal. We next define  $\tilde{\psi}_{u,d}(s) \equiv \int_0^\infty \psi_{u,d}(t) e^{-st} dt$ , and  $\tilde{\phi}_{u,d}(s) \equiv \int_0^\infty \phi_{u,d}(t) e^{-st} dt = [1 - \tilde{\psi}_{u,d}(s)]/s$ . Normalization implies  $\int_0^\infty \psi_{u,d}(t) dt = \tilde{\psi}_{u,d}(0) = 1$ .

The CTRWs can be broadly classified into the stationary and nonstationary walks characterized by finite and infinite mean waiting times  $\bar{t}_{u,d} \equiv \int_0^\infty t \psi_{u,d}(t) dt = \tilde{\phi}_{u,d}(0) = -d\tilde{\psi}_{u,d}(s)/ds|_{s=0}$ , respectively. Nonstationary ensembles generated by power-law  $\psi(t) \propto 1/t^{\alpha+1}$  distributions of fluctuation time scales with divergent  $\bar{t} = \infty$  (i.e.,  $0 < \alpha < 1$ ) [30] are standard *raison d'être* for CTRW model. They show aging (i.e., time-dependent renewal rates or correlation functions) and weak ergodicity breaking, which obscure interpretation of time averages of single molecule experiments by the (commonly calculated) ensemble averages (see Chapter 11 of

Ref. [5]). Some basic concepts of statistical physics must be generalized for this case, such as the relation between the correlation functions and the power spectra (Wiener-Khinchin theorem) [31]. This anomalous power-law behavior was reported, for instance, in power spectrum measurements in CdSe quantum dots [32]. Signatures of nonergodic photon counting statistics of fluorescence blinking from CdSe-ZnS quantum dots are exhibited over any experimental window of practical interest; keeping the true power-law statistics ( $\alpha \approx 0.5$ ) at least for hours [16].

In many experiments, however, the power law spans over limited scale and cutoff turns the walk into the stationary process [33,34] avoiding artificial preparation of the initial state. Another case for the stationary CTRW is power-law WTD with exponent  $\alpha > 1$  [35,36]. Such random walks with  $\bar{\tau} < \infty$  are ergodic and their stationary ensembles can be established [37]. Predictions of time-averaged physical quantities are accessible by averaging over statistical (configuration) ensembles common in statistical physics [38].

Stationary ensemble requires a consistent choice of initial conditions. Observation is started (“initial time”) in an arbitrary moment during the stochastic process. Hence, some time could be already spent from the last jump at the start; the initial time is not a renewal time. The initial conditions must thus include a special WTD for the first jump  $\psi^F(t)$  (different from  $\psi$ ), consistently accounting for all cases found in the stationary ensemble.

Steady-state line shape can only be studied for the stationary noise, when  $\bar{\tau} < \infty$ . It still shows interesting anomalous features, including the breakdown of central limit theorem in photon counting statistics, provided that the power-law exponent is  $1 < \alpha < 2$  [19]. We revisit the stochastic spectral diffusion model of anomalous line shape, but relax the limitations of perturbation theory.

When the anomalous bath dynamics is coupled to a quantum dynamics of a two-level chromophore the steady-state correlations between system and bath are built up. Unlike the Markovian case, the correlation effect is not limited to the system and bath density matrices, but the WTD for the first jump is affected as well. The initial WTD  $\psi_{i,x}^F(t)$  ( $x=u,d$ ) thus shows specific profile for each Liouville space state  $i$ . The consistent prescription for  $\psi_{i,x}^F(t)$  and consequences for the line shapes and photon statistics will be elaborated in the coming sections.

### III. LINE SHAPES

To that end we consider a two-level quantum system (having ground state  $g$  and excited state  $e$ ) whose dynamics include Hamiltonian evolution ( $H_0 = \omega_{eg}(t)|e\rangle\langle e|$ ), spontaneous emission with rate  $\Gamma$ , and dipole interaction with CW laser field ( $H_{int} = -\mathcal{E} \cos(\omega t)|e\rangle\langle g| + h.c.$ ), where  $\mathcal{E}$  is the Rabi frequency. We also set  $\hbar = 1$ . Populations on the ground  $P_g$  and excited states  $P_e$  and coherence (represented by real variables  $\rho'_{eg}, \rho''_{eg}$  in the rotating frame  $\rho_{eg} = e^{i\omega t}[\rho'_{eg} + i\rho''_{eg}]$ ) shall be organized into the vector  $P(t) = (P_e, P_g, \rho'_{eg}, \rho''_{eg})^T$  in the Liouville space, where its time evolution is described by the Bloch equations,

$$\frac{d}{dt} \begin{pmatrix} P_e \\ P_g \\ \rho'_{eg} \\ \rho''_{eg} \end{pmatrix} = \begin{pmatrix} -\Gamma & 0 & 0 & \mathcal{E} \\ \Gamma & 0 & 0 & -\mathcal{E} \\ 0 & 0 & -\Gamma/2 & -\Delta(t) \\ -\mathcal{E}/2 & \mathcal{E}/2 & +\Delta(t) & -\Gamma/2 \end{pmatrix} \begin{pmatrix} P_e \\ P_g \\ \rho'_{eg} \\ \rho''_{eg} \end{pmatrix}. \quad (3)$$

The transition frequency  $\omega_{eg}(t)$  [and the detuning  $\Delta(t) \equiv \omega - \omega_{eg}(t)$ ] jumps between  $\omega_{eg;u} = \omega_0$  and  $\omega_{eg;d} = -\omega_0$  associated with the bath states  $u$  and  $d$ , respectively. The matrix of coefficients (Liouvillean) in Eq. (3) will be hereafter denoted by  $L_u$  and  $L_d$ . We next introduce the *resetting matrix*  $\hat{\Gamma}$  which represents photon emission and transforms  $P(t)$  before the emission into the density after the emission [24],

$$\hat{\Gamma}_u = \hat{\Gamma}_d = \begin{pmatrix} 0 & 0 & 0 & 0 \\ \Gamma & 0 & 0 & 0 \\ 0 & 0 & 0 & 0 \\ 0 & 0 & 0 & 0 \end{pmatrix}. \quad (4)$$

Complete dynamics is represented in the combined Liouville  $\times$  bath space with dimension  $4 \times 2$ . Symbols  $L$  and  $\hat{\Gamma}$  without bath index refer to matrices in this combined space. Hereafter we will use tracing symbol  $\text{Tr}_S$  for summation over the ground- and excited-state densities (1,1,0,0) and  $\text{Tr}_{SB}$  for an additional summation over bath states  $\text{Tr}_{SB} \equiv \sum_{x=u,d} \text{Tr}_S$ .

Model is completed by specifying the steady-state initial condition (including  $\psi^F$ ). Weak field CW line shapes are related by Fourier transform to free-induction decay experiment in time domain. Response function theory follows, in fact, the latter experiment, and calculate the line shape as ground state average [39] of the phase factor

$$I = \text{Re} \int_0^\infty dt e^{-\Gamma t/2} \left\langle \exp \left[ i \int_0^t \Delta(t') dt' \right] \right\rangle_\Delta. \quad (5)$$

The first jump WTD in the ground state  $\psi_g^F$  is (for weak fields) negligibly  $\sim \mathcal{E}^2$  deviated from that of the pure bath dynamics decoupled from the system (see the discussion in Sec. V). The standard prescription for the stationary first jump WTD  $\psi^F(t) = \bar{\tau}^{-1} \int_t^\infty \psi(t') dt'$  [37] thus can be employed. This strategy is inapplicable for strong fields, and the steady-state correlations at  $t=0$  between bath and system must be established by starting the random walk and switching on the electric field at  $t=-\infty$ .

Expanding the strategy explained in Ref. [40] we first calculate the *renewal density*  $\eta_u(t) = (\eta_{e,u}, \eta_{g,u}, \eta'_{eg,u}, \eta''_{eg,u})^T$  [and similarly  $\eta_d(t) = (\eta_{e,d}, \eta_{g,d}, \eta'_{eg,d}, \eta''_{eg,d})^T$ ], the contribution to  $P(t) = (P_e, P_g, \rho'_{eg}, \rho''_{eg})^T$  from bath paths that jumped at time  $t$  to the bath state  $u$  ( $d$ ). Renewal densities  $\eta_{e,u}, \eta_{g,u}$  are simply the densities of bath jumps to  $u$  in the excited and the ground states, respectively. Renewal densities  $\eta'_{eg,u}, \eta''_{eg,u}$  are similar quantities, which measure the amount of coherence  $\rho'_{eg}, \rho''_{eg}$  at the renewal event to state  $u$ . Renewal density serves as a cornerstone for memoryless description disregarding references to past thanks to the renewal property. The steady-state renewal density [in the combined space  $\eta$

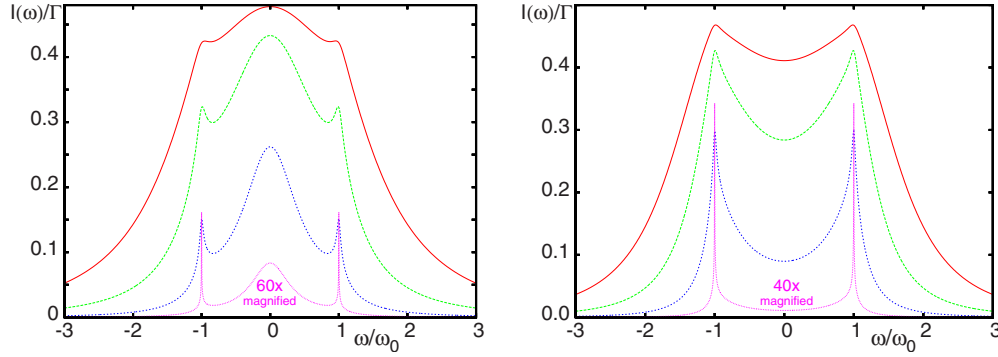


FIG. 1. (Color online) Absorption line shape [Eq. (10)] of the two-level molecule with dichotomic CTRW noise [Eq. (11)] parametrized by  $\alpha=1.5$ ,  $\tau/\bar{\tau}=2/3$ ,  $\Gamma/\omega_0=0.001$  in the fast  $\bar{\tau}\omega_0=0.2$  (left panel) and slow  $\bar{\tau}\omega_0=2.0$  (right panel) fluctuation limits. Weak field line shape  $\mathcal{E}/\Gamma=1$  (violet, dotted line) is magnified (60 times at left and 40 times at right panel), other curves  $\mathcal{E}/\Gamma=20$  (blue, dashed line),  $\mathcal{E}/\Gamma=50$  (green, long-dashed line), and  $\mathcal{E}/\Gamma=100$  (red, solid line) are plotted without rescaling. Spectral random walk corresponds to that of Fig. 1 (middle top and central panel) in Ref. [20], where the weak field line shapes were calculated by using perturbation theory.

$= (\eta_u, \eta_d)$  must be, at any time, reconstructed from the past renewal densities and factor for evolution between the two renewals

$$\eta = \int_{-\infty}^0 \Psi(-t) e^{-Lt} \eta dt. \quad (6)$$

Equation (6) defines the steady-state renewal density up to a normalization factor. The conservation of the total density  $\text{Tr}_{SB} P(t) = \text{Tr}_{SB} \int_0^\infty \Phi(t-t') e^{L(t-t')} \eta(t') dt' = 1$  guarantees existence of the solution to Eq. (6) and implies correct normalization of  $\eta$  by condition  $\sum_{x=u,d} \bar{\tau}_x \text{Tr}_S \eta_x = 1$ .

Equation (6) and the steady-state intensity

$$I = \text{Tr}_{SB} \int_0^\infty \hat{\Gamma} \Phi(t) e^{-Lt} \eta dt \quad (7)$$

are conveniently calculated by using the spectral decomposition of the Liouvillian  $L_x = -\sum_{i=0}^3 \xi_{i,x} \hat{D}_{i,x}$ , into four eigenvalues  $\xi_{i,x}$  ( $i=0, \dots, 3$ ) and associated  $\hat{D}_{i,x}$  (nonorthogonal)  $4 \times 4$  projection matrices ( $\hat{D}_{i,x} \hat{D}_{j,x} = \delta_{ij} \hat{D}_{i,x}$ ) onto their invariant subspace in each bath state  $x=u, d$ . Decomposition will be reconstructed numerically from the left and right eigenvectors of  $L_x$ .

After transforming to the Laplace space [ $\tilde{\Psi}(s-L) \equiv \int_0^\infty \Psi(t) e^{-st+Lt} dt$ ], Eq. (6) reads

$$\eta = \tilde{\Psi}(-L) \eta, \quad (8)$$

and by applying the spectral decomposition and resolving the bath variables, Eq. (8) turns into an eigenvector problem in the Liouville space of  $u$  state,

$$\sum_{i=0}^3 \sum_{j=0}^3 \tilde{\psi}_d(\xi_{i,d}) \tilde{\psi}_u(\xi_{j,u}) \hat{D}_{i,d} \hat{D}_{j,u} \eta_u = \eta_u. \quad (9)$$

The renewal density in the  $d$  state is then

$$\eta_d = \sum_{j=0}^3 \tilde{\psi}_u(\xi_{j,u}) \hat{D}_{j,u} \eta_u,$$

and Eq. (7) becomes

$$I(\omega) = \sum_{i=0}^3 \sum_{x=u,d} \tilde{\phi}_x(\xi_{i,x}) \text{Tr}_S[\hat{\Gamma}_x \hat{D}_{i,x} \eta_x]. \quad (10)$$

Figure 1 demonstrates the effect of a strong laser field on anomalous line shapes. Anomalous spectral jumps between the fundamental frequencies  $\omega_{eg} = \pm \omega_0$  are implemented by using power-law ( $\psi(t) \sim 1/t^{\alpha+1}$ ) WTD,

$$\tilde{\psi}_u(s) = \tilde{\psi}_d(s) = \frac{1}{1 + \bar{\tau}s/[1 + (\tau s)^{\alpha-1}]}; \quad 1 < \alpha < 2. \quad (11)$$

Two regimes of spectral random walk distinguish whether typical waiting time  $\bar{\tau}$  is sufficiently long to resolve difference between transition frequencies  $\sim 2\omega_0$ . Line shapes of the slow fluctuation regime ( $\bar{\tau}\omega_0 \gg 1$ ) consist of two sharp peaks at fundamental frequencies  $\omega = \pm \omega_0$  (right panel in Fig. 1). Peaks represent bath trajectories with long periods of persistent behavior. Such periods are always present in anomalous CTRW dynamics regardless of parametrization, measured by the survival function of the first jump  $\phi^f$ . So, the  $\omega = \pm \omega_0$  peaks are identified even in fast fluctuation ( $\bar{\tau}\omega_0 \ll 1$ ) line shape (left panel), in contrast to Markovian spectral diffusion, where similar peaks disappear in the fast limit [41]. Periods of fast diffusive motion are represented in the fast fluctuation ( $\bar{\tau}\omega_0 \ll 1$ ) line shapes by an additional motional narrowing peak at the central frequency.

Good qualitative agreement with the perturbation theory is obtained in the weak field regime (violet dotted line), except that the singular analytical peak structure  $I \approx (\omega \pm \omega_0)^\alpha$  predicted by perturbation theory [19] for  $\Gamma=0$  cannot be fully reproduced [42]. Correct account of the steady-state system-bath correlations do not affect weak field line shapes too much because dominant occupation of the ground level

implies small correlations in ground state  $\psi_g^F$  (as will be demonstrated in Sec. V) and assumptions of the perturbation theory are thus satisfied.

When the intensity of laser field is increased beyond the weak field limit, the saturation broadening  $\sim \mathcal{E}$  is identified on all peaks as dominant contribution to the peak width for  $\mathcal{E} \gg \Gamma$  line shapes (blue dashed, green long-dashed, and red solid lines in Fig. 1). Finite laser fields  $\mathcal{E}$  also suppress the  $I \propto (\omega - \omega_0)^\alpha$  singularity reported in Ref. [19]; however, the two peaks at fundamental frequencies  $\omega = \pm \omega_0$  remain rather sharp unless the transition is nearly saturated at  $\mathcal{E} = 100\Gamma$  (red solid line).

#### IV. PHOTON COUNTING STATISTICS

Next we inspect the photon counting statistics. To that end we introduce the propagator  $\Sigma(t)$ , matrix in the combined space, whose  $\Sigma_{ix,jy}(t)$  element is the conditional density that system renewed in bath state  $y=u,d$  (and residing in the Liouville space state  $j=e,g,eg',eg''$ ) at some arbitrary time  $t_a$  will be renewed again after time  $t$  (i.e., at  $t_a+t$ ) to bath state  $x$  in the Liouville space state  $i$ . During the interval arbitrary number of bath jumps and any Liouville space dynamics can occur. Propagator is constructed in analogy with Eq. (6) [40],

$$\Sigma(t) = \delta(t) + \int_0^t \Psi(t-t') e^{L(t-t')} \Sigma(t') dt'. \quad (12)$$

Equation (12) is conveniently solved in the Laplace space  $\tilde{\Sigma}(s) = [1 - \tilde{\Psi}(s-L)]^{-1}$ . The bath space indices can be readily resolved yielding the Liouville space blocks

$$[\tilde{\Sigma}(s)]_{uu} = \left[ 1 - \sum_{ij=0}^3 \tilde{\psi}_d(s + \xi_{i,d}) \tilde{\psi}_u(s + \xi_{j,u}) \hat{D}_{i,d} \hat{D}_{j,u} \right]^{-1},$$

$$[\tilde{\Sigma}(s)]_{du} = \sum_{j=0}^3 \tilde{\psi}_u(s + \xi_{j,u}) \hat{D}_{j,u} [\tilde{\Sigma}(s)]_{uu}. \quad (13)$$

Blocks  $[\tilde{\Sigma}(s)]_{dd}$  and  $[\tilde{\Sigma}(s)]_{ud}$  are implied by interchange of indices  $u$  and  $d$  in Eq. (13).

With Eq. (13) we are ready to calculate the joint probability to detect photons at two times, 0 and  $t$  (two-point correlation function). We follow dynamics from the steady state at the time of the last jump  $t_-$  before the first detection. We sort the bath paths into two groups: the first one [see Fig. 2, (i)] includes the bath paths which have at least one jump between the two detections at 0 and  $t$ , and the other one has no jump [see Fig. 2, (ii)]. In the former case we consider times  $t_1$  and  $t-t_2$  of the first and the last jumps in the interval  $(0, t)$ , respectively. The dynamics between times  $-t_-, 0$  is described by factor  $e^{Lt_-}$ , the emission at  $t=0$  by resetting matrix  $\hat{\Gamma}$ , the evolution between 0 and  $t_1$  by matrix  $e^{Lt_1}$ , and the jump at  $t_1$  by matrix  $\Psi(t_1+t_-)$ . The propagation between  $t_1$  and  $t-t_2$ , including all jumps, is described by  $\Sigma(t-t_1-t_2)$ . The final evolution is accounted by  $\Phi(t_2)e^{Lt_2}$ , and  $\hat{\Gamma}$  stands for the second emission. The latter contribution [Fig. 2, (ii)] shows no bath dynamics and we can follow standard theory of pho-

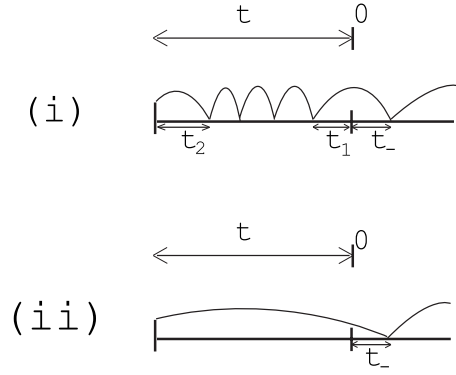


FIG. 2. Contributions from two types of bath trajectories are calculated separately in Eq. (14). Bath jumps are depicted as intersections of the curve with the time axis. The (i) diagram represents all bath paths with at least one bath jump between the two emissions. In the (ii) diagram no jump occurs between the two emission at 0 and  $t$ . Ground line is time axis (time goes from right to left), bath jumps are depicted as intersections of the curve with the time axis.

ton counting [24], except the final convolution with the survival function  $\Phi$ . The two-point correlation function is finally obtained by integrating over possible  $t_-, t_1, t_2$

$$g^{(2)}(t) = \int_0^t dt_2 \int_0^{t-t_2} dt_1 \int_0^\infty dt_- \text{Tr}_{SB}[\hat{\Gamma} \Phi(t_2) \times e^{Lt_2} \Sigma(t-t_1-t_2) \Psi(t_1+t_-) e^{Lt_1} \hat{\Gamma} e^{Lt_-} \eta] + \int_0^\infty dt_- \text{Tr}_{SB}[\Phi(t+t_-) \hat{\Gamma} e^{Lt} \hat{\Gamma} e^{Lt_-} \eta]. \quad (14)$$

Equation (14) has a natural convolution structure. The integrations can be carried out in the Laplace space, and taking the summations over bath index explicitly, we get Liouville space formula

$$\tilde{g}^{(2)}(s) = \sum_{ijk=0}^3 \sum_{xyz=u,d} \tilde{\phi}_y(s + \xi_{k,y}) \frac{\tilde{\psi}_x(s + \xi_{j,x}) - \tilde{\psi}_x(\xi_{i,x})}{s + \xi_{j,x} - \xi_{i,x}} \times (1 - \delta_{zx}) \text{Tr}_S[\hat{\Gamma}_y \hat{D}_{k,y} \Sigma_{y,z}(s) \hat{D}_{j,x} \hat{\Gamma}_x \hat{D}_{i,x} \eta_x] + \sum_{x=u,d} \sum_{ij=0}^3 \frac{\tilde{\phi}_x(s + \xi_{j,x}) - \tilde{\phi}_x(\xi_{i,x})}{s + \xi_{j,x} - \xi_{i,x}} \times \text{Tr}_S[\hat{\Gamma}_x \hat{D}_{j,x} \hat{\Gamma}_x \hat{D}_{i,x} \eta_x], \quad (15)$$

suitable for implementation.

Numerical inverse Laplace transform of Eq. (15) was used to calculate the two-point correlation function shown in Fig. 3. Short time antibunching  $g^{(2)} < I^2$  represents the erasure of coherence during photon emission. Bunching  $g^{(2)} > I^2$  at later times is normally caused by either Rabi oscillations or the correlation between bath and Liouville space populations. CTRW spectral diffusion has an additional source of bunching in the steady-state correlation of the initial WTD and the Liouville space state. Memory is manifested at fundamental frequencies  $\omega = \pm \omega_0$  (left panel),

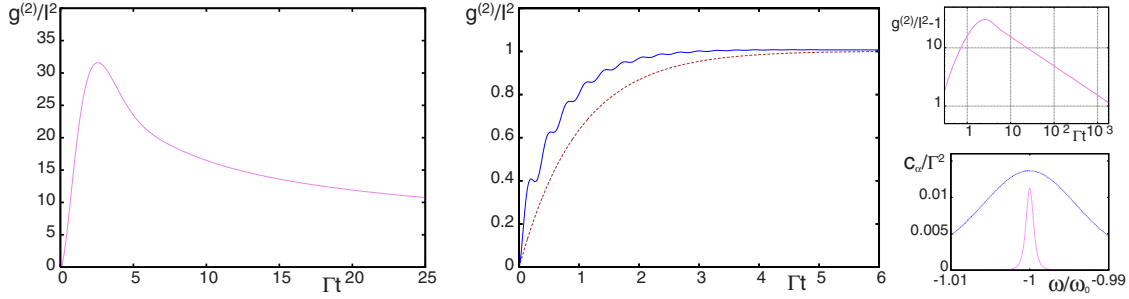


FIG. 3. (Color online) Two-point correlation function  $g^{(2)}(t)$  [Eq. (10)] of the system in Fig. 1, fast bath limit  $\alpha=1.5$ ,  $\tau/\bar{\tau}=2/3$ ,  $\Gamma/\omega_0=0.001$ ,  $\bar{\tau}\omega_0=0.2$ . Left: Weak laser field  $\mathcal{E}/\Gamma=1$  tuned on the transition frequency of the  $u$  state  $\Delta_u=0.0$ ,  $\Delta_d=2.0$  (violet, solid line) Central: Increased magnitude of field  $\mathcal{E}/\Gamma=20$  (blue, solid line) or tuning on the central peak  $\Delta_u=-1.0$   $\Delta_d=1.0$  (brown, dashed line) reduces the bunching. Right top: Linearity of log-log plot proves the power-law asymptotic decay of  $g^{(2)}(t)/I^2-1$  for the system of the left panel  $\mathcal{E}/\Gamma=1$ ,  $\Delta_u=0.0$ ,  $\Delta_d=2.0$ . Right bottom: Coefficient  $c_\alpha$  [Eq. (16)] of asymptotic power-law growth of the Mandel  $Q$  parameter as a function of frequency. Peak around the transition frequency  $\omega \approx -\omega_0$  is shown for the weak  $\mathcal{E}/\Gamma=1$  (violet, solid) and strong  $\mathcal{E}/\Gamma=20$  (blue, dotted) laser field.

while at the central peak, backed by fast fluctuations, bunching does not show up (central panel, dashed line). The correlation function shows anomalous power-law decay (top right panel)  $g^{(2)}(t)=g^{(2)}(\infty)+c_\alpha/t^{\alpha-1}$  toward its asymptotic value  $g^{(2)}(\infty)=I^2$  [43].

Another measure of photon count, the Mandel  $Q$  parameter  $Q(T) \equiv (\langle N^2 \rangle - \langle N \rangle^2) / \langle N \rangle$ , characterizes statistical distributions of photon count  $N$  binned over time window  $T$ . In most cases, (e.g., when spectral diffusion is Markovian, or for  $\alpha > 2$ ) the distribution of photons approaches the Gaussian statistics with  $T \rightarrow \infty$  and constant asymptotic value of Mandel  $Q$  parameter characterizes the deviation of variance from the Poissonian statistics of emission [44]. The breakdown of central limit theorem is signified by asymptotically growing Mandel  $Q$  parameter. Ballistic  $Q(T) \propto T$  (for  $0 < \alpha < 1$ ) and power-law  $Q(T) \propto T^{2-\alpha}$  (for  $1 < \alpha < 2$ ) expansions of Mandel  $Q$  parameter has been studied for aging random walks of fluorescent intensities [19] and the ballistic case was already observed in fluorescence from CdSe-ZnS quantum dots [16]. Since  $Q(T) = (IT)^{-1} \int_0^T \int_0^t [g^{(2)}(t'') - I^2] dt'' dt'$  [21], coefficient  $c_\alpha$  determines the asymptotic growth of Mandel  $Q$  parameter for stationary random walks [Eq. (11)],

$$Q(T) \approx \frac{c_\alpha T^{2-\alpha}}{(2-\alpha)(3-\alpha)I}.$$

Numerical costs of inverse Laplace transform can be avoided in the Laplace space, where  $c_\alpha$  can be deduced from  $s \rightarrow 0$  asymptotic expansion  $\tilde{g}^{(2)}(s) = g^{(2)}(\infty)/s + c_\alpha \gamma(2-\alpha)s^{\alpha-2}$ , where  $\gamma(z) \equiv \int_0^\infty x^{z-1} e^{-x} dx$  is the Gamma function. Term  $g^{(2)}(\infty)$  does not enter when inspecting imaginary part of  $s\tilde{g}^{(2)}(s)$  along some line  $s = |s|e^{i\varphi}$  ( $\varphi$  is fixed) in complex plane,

$$\text{Im } s\tilde{g}^{(2)}(s) \approx c_\alpha \gamma(2-\alpha) \sin[\varphi(\alpha-1)] |s|^{\alpha-1} \quad (16)$$

Frequency profile of  $c_\alpha$  has only two symmetric very sharp peaks at fundamental frequencies  $\omega = \pm \omega_0$ , but no peak at the central frequency even in the fast fluctuation limit. The peak at  $\omega = -\omega_0$  is shown at the right bottom panel of Fig. 3 for two magnitudes of the laser field corresponding to line shapes of Fig. 1, left. Peaks of Mandel  $Q$  parameter become

weaker (relatively to  $I$ ) and less sharp with increasing magnitude of the laser field. These results can be understood as a picture of periods of rapid bath fluctuations and persistence during anomalous spectral diffusion [40,45]. The former periods are responsible for the central peak of  $I$  spectrum (Fig. 1) and do not carry memory responsible for asymptotic growth of Mandel parameter. The other peaks of  $I$  spectrum are caused by the persistent periods, and thus are represented in  $c_\alpha$  spectrum. The asymptotic Mandel  $Q$  parameter can thus help to distinguish between peaks of spectra of different origin. Our observation is consistent with 2D line shapes of coherent nonlinear spectroscopy—another four-point dipole correlation probe. Periods of both types are simultaneously represented in the single molecule spectrum and the 2D spectrum by the static and the motionally narrowed peaks and only the former carry anomalous peak dynamics [40]. Saturation effects make the spectral lines less resolved and suppress system-bath correlations because the occupation of the ground and excited states becomes alike for any detuning  $\Delta(t)$ .

Presented algorithm can be easily extended to the multi-point correlation functions  $g^{(k)}$ . The bath paths shall be classified in the spirit of Ref. [40] (see Figs. 3 and 4 therein) and the algorithm for constructing many-interval response functions should be adapted to account for more general dynamics  $L$ , such as treated here, for the factor of the photon emission  $\hat{\Gamma}$  and for the steady-state initial condition Eq. (6) in the way explained earlier in this section. Higher,  $k$ th factorial moment  $F^{(k)} \equiv \langle N(N-1)\dots(N-k+1) \rangle$  of photon counting statistics  $F^{(k)}$  can be obtained by integrating out the correlation function (see Chapter 4 of Ref. [5] for details), yielding the Laplace space formula

$$\tilde{F}^{(k)}(s) = \frac{k!}{s^2} \tilde{g}^{(k)}(s, s, \dots, s). \quad (17)$$

The full counting statistics shall be calculated by straightforward implementation of the generating function approach [24] to our algorithm. For the evolution during binning interval  $0, T$  the Liouvillian should be standardly replaced by  $L^\zeta = L + (e^{i\zeta} - 1)\hat{\Gamma}$ , where  $\zeta$  is an auxiliary variable. Evolution

at earlier times and the calculation of the steady state  $\eta$  [Eq. (6)] remains unaffected, and represented by  $L$  [46]. The generating function reads

$$G(T, \zeta) = \int_0^T dt_2 \int_0^{t-t_2} dt_1 \int_0^\infty dt_- \text{Tr}_{SB} \Phi(t_2) \times e^{L\zeta t_2} \sum_{\xi} \xi(t-t_1-t_2) \Psi(t_1+t_-) e^{L\zeta t_1} e^{L t_-} \eta + \int_0^\infty dt_- \text{Tr}_{SB} \Phi(t+t_-) e^{L\zeta t} e^{L t_-} \eta \quad (18)$$

and can be transformed to photon count distribution by  $C(T, N) = \int_0^{2\pi} G(T, \zeta) e^{-i\zeta N} d\zeta$ .

### V. STEADY-STATE DISTRIBUTIONS OF THE FIRST SPECTRAL JUMP

Our consistent (steady-state) choice of initial state [Eq. (6)] makes the difference against the perturbation approaches of Refs. [19,20] based on the ground-state dipole correlation functions. Traditionally, the initial condition is set up by specifying  $\psi^F$ . Thus we will construct the steady-state initial WTDs in the ground and excited states explicitly.

To that end we introduce the projector  $\mathcal{P}_e$  onto the excited and  $\mathcal{P}_g$  onto the ground state, represented in the Liouville space by matrices

$$\mathcal{P}_e = \begin{pmatrix} 1 & 0 & 0 & 0 \\ 0 & 0 & 0 & 0 \\ 0 & 0 & 0 & 0 \\ 0 & 0 & 0 & 0 \end{pmatrix}, \quad \mathcal{P}_g = \begin{pmatrix} 0 & 0 & 0 & 0 \\ 0 & 1 & 0 & 0 \\ 0 & 0 & 0 & 0 \\ 0 & 0 & 0 & 0 \end{pmatrix}.$$

Following the above explained principles we find the WTD for the first jump  $\psi_{ix}^F$  from the bath state  $x=u, d$  at the molecular state  $i=e, g$  to be

$$\psi_{ix}^F(t) = \frac{\sum_{j=0}^3 \text{Tr}_S \mathcal{P}_i \hat{D}_{j,x} \eta_x \int_0^\infty \psi_x(t+t') e^{-\xi_j t'} dt'}{\sum_{k=0}^3 \tilde{\phi}_x(\xi_{k,x}) \text{Tr}_S \mathcal{P}_i \hat{D}_{k,x} \eta_x}. \quad (19)$$

Denominator of Eq. (19) is the steady state density of particles in the  $ix$  state, and ensures correct normalization  $\int_0^\infty \psi_{ix}^F(t) dt = 1$ . Equation (19) and power-law tailed WTDs  $\psi_u = \psi_d \propto (\tau/t)^{\alpha+1}$  were used to plot Fig. 4. Figure 4 documents the different steady-state distribution of waiting times for the first spectral jump in the excited state and in the ground state of the two-level molecule at rather weak laser fields. Ground-state WTDs  $\psi_{gu}^F$  and  $\psi_{gd}^F$  do not differ significantly from  $\psi_x^F(t) = \tau^{-1} \int_0^\infty \psi_x(t') dt'$  ( $x=u, d$ ), the total first jump WTD from  $u$  for weak laser fields. Weighted sum of WTDs  $\psi_{eu}^F$  and  $\psi_{gu}^F$  must correspond to  $\psi_u^F(t)$ , i.e.,  $P_{eu} \psi_{eu}^F + P_{gu} \psi_{gu}^F = [P_{eu} + P_{gu}] \psi_u^F(t)$ , and since  $P_{eu} \rightarrow 0$  in the weak field limit,  $\psi_{gu}^F \rightarrow \psi_u^F(t)$ . The replacement of  $\psi_{gu}^F, \psi_{gd}^F$  by  $\psi^F(t)$  is thus justified for weak field line shapes. The excited-state WTDs (significant for the two-point correlation function  $g^{(2)}$ ), on the other hand, show large deviations from  $\psi^F(t)$ ,

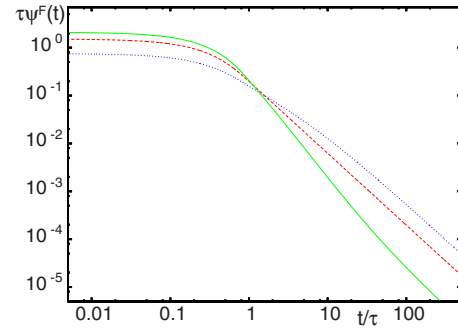


FIG. 4. (Color online) Initial WTD [Eq. (19)] in the excited state  $\psi_{eu}^F$  (blue dotted line),  $\psi_{ed}^F$  (green solid line), and in the ground state  $\psi_{gd}^F \approx \psi_{gu}^F \approx \psi^F$  (red dashed line) are plotted for power-law WTD  $\psi_u(t) = \psi_d(t) \propto (\tau/t)^{\alpha+1}$  at long times ( $t > 1$ ) with an early ( $t < 1$ ) exponential onset  $\psi_u(t) = \psi_d(t) \propto e^{(\alpha+1)(1-t/\tau)}$ . Parameters:  $\Gamma = 1$ ,  $\mathcal{E}/\Gamma = 0.1$ ,  $\Delta_d/\Gamma = 5.0$ ,  $\Delta_u/\Gamma = -0.01$ , and  $\alpha = 1.5$ .

consistent with the picture of persistent periods discussed above. Laser at resonance with transition frequency of bath state  $d$  makes the excited-state population mostly contributed from the paths persisting at  $d$ . Since the persistent particles have also delayed expectations of coming jump,  $\psi_{ed}^F$  shows significantly longer tails than  $\psi_{eu}^F, \psi_{gd}^F$ , or  $\psi_{gu}^F$ . Complex time profiles of Fig. 4 reflect changing proportion between  $\xi_j \neq 0$  contributions  $\int dt' e^{-\xi_j t'} / (t+t')^{\alpha+1} \propto 1/\xi_j t^{\alpha+1}$  and  $\xi_0 = 0$  contribution  $\int dt' 1/(t+t')^{\alpha+1} \propto 1/t^\alpha$  to the nominator of Eq. (19). Increased magnitude of the laser field tends to suppress the correlation effect in the excited state. Weak field theory of two-point correlation function would thus rather overestimate the correlation effects. In other words, the bath correlations show up more sensitively for weak fields as we have documented at Fig. 3 for Mandel  $Q$  parameter.

Some useful insights could be naively expected by introducing projection  $\mathcal{P}_{eg}$  on the  $eg$  coherence matrix element. However, while  $\psi_{e,x}^F, \psi_{g,x}^F$  can be unambiguously interpreted as the initial WTDs, different  $\psi^F$  are predicted for the real  $\rho'_{eg}$  and the imaginary part  $\rho''_{eg}$  of the coherence by Eq. (19). The correlation effect cannot be described in terms of initial WTDs for the coherence matrix element.

We should address how quickly is the steady-state (6) built up when the electric field is switched on at finite time before detection. Most effects of switching on the electric field are relaxed at  $\sim \Gamma^{-1}$  time scale. Nevertheless, rebuild of  $\psi_{ix}^F$  to a new steady state (different from that of  $\mathcal{E}=0$ ) also induces some long-lived component, with time profile similar to bath relaxation. So, the steady state is approached with  $1/t^{\alpha-1}$  power law decay for WTD of Eq. (11). This may seem to obscure some of our asymptotic conclusion. They are, however, correct in the following sense: Predicted asymptotic power-law decays are relevant for shorter (future) times than the time elapsed from the laser switch on.

In conclusion, we generalized theory of anomalous line shapes to arbitrarily strong driving fields, where the initial steady-state correlation between the Liouville space and bath space dynamics must be accounted for. We revisited line shapes and photon counting statistics of the two-level chromophore with CTRW dichotomic noise, and showed frequency profiles of asymptotic growth of Mandel parameter

(related to non-Gaussian photon statistics) at steady state formed by applying laser field of arbitrary magnitude. Microscopic picture of anomalous spectral diffusion drawn by the photon counting statistics is consistent with that drawn by the multidimensional line shapes of coherent nonlinear spectroscopy. Ensembles (or sufficiently long single molecule bath trajectories) show both signatures of fast fluctuating particles (motional narrowing) and the fraction of particles persisting for long time in the same bath state. Asymptotic Mandel parameter identifies peaks at fundamental bath frequencies, which are related to the persistent behavior, and can help to discriminate between microscopi-

cally nonequivalent models with similar absorption spectrum [47].

#### ACKNOWLEDGMENTS

The support of the Grant Agency of the Czech Republic (Grant No.202/07/P245), and the Ministry of Education of the Czech Republic (research program MSM Grant No. 0021620835) is gratefully acknowledged. The author is indebted to Dr. Tomáš Novotný for careful reading of this manuscript.

- 
- [1] O. Flomenbom, K. Velonia, D. Loos, S. Masuo, M. Cotlet, Y. Engelborghs, J. Hofkens, A. E. Rowan, R. J. M. Nolte, F. C. de Schryver, and J. Klafter, *Proc. Natl. Acad. Sci. U.S.A.* **102**, 2368 (2005).
- [2] Th. Basché, S. Kummer, and C. Bräuchle, *Nature (London)* **373**, 132 (1995).
- [3] C. Hettich, C. Schmitt, J. Zitzmann, S. Kühn, I. Gerhardt, and V. Sandoghar, *Science* **298**, 385 (2002).
- [4] M. Lippitz, C. G. Hübner, T. Christ, H. Eichner, P. Bordat, A. Herrmann, K. Müllen, and T. Basché, *Phys. Rev. Lett.* **92**, 103001 (2004).
- [5] *Theory and Evaluation of Single-Molecule Signals*, edited by E. Barkai, F. L. H. Brown, M. Orrit, and H. Yang (World Scientific, Singapore, 2008).
- [6] I. S. Osad'ko, *Selective Spectroscopy of Single Molecules* (Springer, Berlin, 2002).
- [7] M. Kuno, D. P. Fromm, S. T. Johnson, A. Gallagher, and D. J. Nesbitt, *Phys. Rev. B* **67**, 125304 (2003).
- [8] H. Yang, G. Luo, P. Karnchanaphanurach, T.-M. Louie, I. Rech, S. Cova, L. Xun, and X. S. Xie, *Science* **302**, 262 (2003).
- [9] J. P. Hoogenboom, E. M. H. P. van Dijk, J. Hernando, N. F. van Hulst, and M. F. García-Parajó, *Phys. Rev. Lett.* **95**, 097401 (2005).
- [10] R. Granek and J. Klafter, *Phys. Rev. Lett.* **95**, 098106 (2005).
- [11] F. Cichos, C. von Borczyskowski, and M. Orrit, *Curr. Opin. Colloid Interface Sci.* **12**, 272 (2007).
- [12] A. L. Efros and M. Rosen, *Phys. Rev. Lett.* **78**, 1110 (1997).
- [13] P. Frantsuzov, M. Kuno, B. Jánko, and R. A. Marcus, *Nat. Phys.* **4**, 519 (2008).
- [14] S. C. Kou and X. S. Xie, *Phys. Rev. Lett.* **93**, 180603 (2004).
- [15] X. Brokmann, J. P. Hermier, G. Messin, P. Desbiolles, J.-P. Bouchaud, and M. Dahan, *Phys. Rev. Lett.* **90**, 120601 (2003).
- [16] G. Margolin, V. Protasenko, M. Kuno, and E. Barkai, *J. Phys. Chem. B* **110**, 19053 (2006).
- [17] O. Flomenbom and R. Silbey, *Proc. Natl. Acad. Sci. U.S.A.* **103**, 10907 (2006).
- [18] J. P. Hoogenboom, J. Hernando, M. F. García-Parajó, and N. F. van Hulst, *J. Phys. Chem. C* **112**, 3417 (2008).
- [19] Y. Jung, E. Barkai, and R. Silbey, *Chem. Phys.* **284**, 181 (2002).
- [20] F. Šanda and S. Mukamel, *Phys. Rev. E* **73**, 011103 (2006).
- [21] L. Mandel, *Opt. Lett.* **4**, 205 (1979).
- [22] R. J. Cook, *Phys. Rev. A* **23**, 1243 (1981).
- [23] D. Lenstra, *Phys. Rev. A* **26**, 3369 (1982).
- [24] F. L. H. Brown, *Acc. Chem. Res.* **39**, 363 (2006).
- [25] Y. He and E. Barkai, *Phys. Rev. Lett.* **93**, 068302 (2004).
- [26] Y. Tanimura, *J. Phys. Soc. Jpn.* **75**, 082001 (2006).
- [27] I. Goychuk and P. Hänggi, *Phys. Rev. Lett.* **91**, 070601 (2003).
- [28] G. Gangopadhyay and Y. Tanimura, *Chem. Phys. Lett.* **289**, 97 (1998).
- [29] A. I. Shushin, *Phys. Rev. E* **67**, 061107 (2003).
- [30] J. Klafter, M. F. Shlesinger, and G. Zumofen, *Phys. Today* **49**(2), 33 (1996).
- [31] G. Margolin and E. Barkai, *J. Stat. Phys.* **122**, 137 (2006).
- [32] M. Pelton, D. G. Grier, and P. Guyot-Sionnest, *Appl. Phys. Lett.* **85**, 819 (2004).
- [33] R. Verberk and M. Orrit, *J. Chem. Phys.* **119**, 2214 (2003).
- [34] I. Chung, J. B. Witkoskie, J. Cao, and M. G. Bawendi, *Phys. Rev. E* **73**, 011106 (2006).
- [35] F. Šanda and S. Mukamel, *Phys. Rev. Lett.* **98**, 080603 (2007).
- [36] G. Aquino, L. Palatella, and P. Grigolini, *Phys. Rev. Lett.* **93**, 050601 (2004).
- [37] W. Feller, *An Introduction of Probability Theory and Its Applications* (Wiley, New York, 1968), Vol. 1.
- [38] To overcome technical choice  $\psi^F = \psi$  common in most literature instead of proper choice Eq. (19), note that the initial period to the first jump only affects  $T^{-1} \int_0^T \phi^F(t) dt \approx T^{1-\alpha}$  part of the measured quantity. Its contribution to the time averages thus vanishes in  $T \rightarrow \infty$  limit.
- [39] S. Mukamel, *Principles of Nonlinear Optical Spectroscopy* (Oxford University Press, New York, 1995).
- [40] F. Šanda and S. Mukamel, *J. Chem. Phys.* **127**, 154107 (2007).
- [41] R. Kubo, in *Fluctuation, Relaxation and Resonance in Magnetic Systems*, edited by D. ter Haar (Oliver and Boyd, Edinburgh, 1962) p. 23.
- [42] Choice  $\Gamma=0$  is inconsistent in the model Eqs. (3) and (4). Therefore, peaks are regularized by finite  $\Gamma, \mathcal{E}$ . Awkward limiting procedure necessary for obtaining  $\Gamma=0$  line shape in the weak field limit  $\lim_{\Gamma \rightarrow 0} \lim_{\mathcal{E} \rightarrow 0} \mathcal{E}^{-2} I(\omega, \Gamma, \mathcal{E})$  provides only pointwise convergence to the line shape of response function theory. It is thus impossible to approach the singularity at  $\omega = \pm \omega_0$  peaks by parametrization of the model [Eq. (3)] within specified error.
- [43] Relation holds, since  $\tilde{\Sigma}(s \rightarrow 0) \rightarrow s^{-1} \eta \text{Tr}_{SB} \tilde{\Phi}(L)$ .
- [44] H. F. Arnoldus and G. Nienhuis, *Opt. Acta* **30**, 1573 (1983).
- [45] F. Šanda and S. Mukamel, *Phys. Rev. E* **72**, 031108 (2005).
- [46] F. Šanda and S. Mukamel, *Phys. Rev. A* **71**, 033807 (2005).
- [47] M. Olszewski and N. A. Sergeev, *Z. Naturforsch., A: Phys. Sci.* **63**, 688 (2008).